Supplemental information

Phase diagrams, thermodynamic properties and sound velocities derived from a multiple Einstein method using Vibrational Densities of States: An application to MgO-SiO_2

Michael HG Jacobs, Institute of Metallurgy, Clausthal University of Technology, Robert-Koch Str 42, 38678 Clausthal-Zellerfeld, Germany
Email: Michael.Jacobs@TU-Clausthal.de

Rainer Schmid-Fetzer, Institute of Metallurgy, Clausthal University of Technology, Robert-Koch Str 42, 38678 Clausthal-Zellerfeld, Germany

Arie P van den Berg, Dept. Theoretical Geophysics, Utrecht University, Budapestlaan 4, 3584 CD, Utrecht, The Netherlands

Physics and Chemistry of Minerals

This section gives details of thermodynamic analyses of each substance separately.

Heat capacities

The vibrational frequencies at zero Kelvin and zero pressure and shape of the VDoS dominantly determine the isochoric heat capacity. The right-hand side frames in Figure 3, especially the inset frames, illustrate for wadsleyite and ringwoodite that at low temperature this property is insignificantly different from the experimental isobaric heat capacity. Figure 3 also shows that experimental isobaric heat capacity data above room temperature measured by Ashida et al. (1987) and Watanabe (1982) are systematically below our calculated isochoric heat capacity curves. That indicates that these measurements are likely to be inaccurate. Our present results for heat capacity are not significantly different from those of Jacobs and de Jong (2007) who used a VDoS derived from Raman and Infrared spectroscopic data and Kieffer's (1979) model, indicating that vibrational models produce robust results. Additionally, although we used intrinsic anharmonicity in our description for the lattice vibrations of wadsleyite, its effect on isobaric and isochoric heat capacity is insignificant in the temperature range of Figure 3. Kojitani et al. (2012), investigating ringwoodite and, referring to a canonical paper of Mraw and Naas (1979), showed that the calorimetric measurements of Ashida et al. (1987) and Watanabe (1982), performed with a scanning method, are less accurate than their own calorimetric measurements, performed with an enthalpy method. The measurements of Kojitani et al. (2012) and the measurements of Jahn et al. (2013), who followed the same calorimetric method as Kojitani et al. (2012) but for wadsleyite, are larger than our calculated isochoric heat capacity curves and therefore more reliable than those of Ashida et al. (1987) and Watanabe (1982). Because the VDoS, i.e frequencies and fractions in our method, predominantly determines the isochoric heat capacity, knowledge of bulk modulus, thermal expansivity and volume is not required to conclude if isobaric heat capacity data are above or below the calculated isochoric heat capacity curve. This feature of combining low-temperature heat capacity data and an accurate VDoS in our method is a powerful tool to indicate whether or not a particular heat capacity data set can be reliably used in a thermodynamic analysis.

We applied the same method to akimotoite, illustrated in the upper-left frame of "online resource, Figure 2", by using the VDoS of Karki and Wentzcovitch (2002) to calculate the isochoric heat capacity. We arrived at the same conclusion that isobaric heat capacity measured by Ashida et al. (1987) and Watanabe (1982) are below our calculated isochoric heat capacity. Although no other heat capacity measurements are available above room

temperature we assumed in the phase diagram analysis that these measurements are flawed in the same way as for wadsleyite and ringwoodite. For perovskite, shown in the upper-right frame of "online resource Figure 2", we found in the same way that the VDoS of Karki et al. (2000a) is consistent with the low-temperature heat capacity measurements of Akaogi et al. (2008), which are significantly above the DSC measurements of Akaogi et al. (1993). For this substance no heat capacity measurements are available above room temperature. High-temperature heat capacity behaviour is constrained by accurate *V-P-T* data, recently measured by Katsura et al. (2009) and depicted in the upper-right frame of Figure 4. High-temperature heat capacity is not significantly different from that calculated by Jacobs and de Jong (2007) and Chopelas (2000).

For stishovite we found that the VDoS predicted by Oganov et al. (2005) is consistent with the low-temperature heat capacity data of Yong et al. (2012) and Akaogi et al. (2011). "Online resource, Figure 2" illustrates that these data are also consistent with high-temperature heat capacity data of Akaogi et al. (1995) and Yusa et al. (1993). For the $CaCl_2$ form of SiO_2, stable at pressures above about 50 GPa, no heat capacity data are available, and its description is constrained by ab initio predictions of Oganov et al. (2005). Above about 80 GPa the α-PbO_2 form of SiO_2, also named columbite, and which we abbreviate as St-II in Table 2, becomes stable. Heat capacity is constrained by the VDoS predicted by Oganov et al. (2005).

For the post-perovskite and high-pressure clinoenstatite forms of $MgSiO_3$ no heat capacity data are available because they cannot be quenched to ambient pressure conditions. We constrained heat capacities for these polymorphs by the predicted VDoS of Tsuchiya et al. (2005) and Choudhury and Chaplot (2000) respectively.

For the majorite form of $MgSiO_3$ only data from Yusa et al. (1993) measured by DSC are available and these appear to be consistent with the VDoS of Yu et al. (2011).

For the low-pressure clino enstatite form of $MgSiO_3$ only low-temperature heat capacity data from Drebushchak et al. (2008) are available established by adiabatic calorimetry. "Online resource, Figure 2" shows that these data are consistent with the VDoS predicted by Yu et al. (2010).

Forsterite, wadsleyite and ringwoodite

We treated forsterite in Jacobs et al. (2013) without dispersion in Grüneisen parameters and noticed that replacing the VDoS of Price et al. (1987) by that predicted by Li et al. (2007) did not change the results significantly. Due to monodispersion in the Grüneisen parameters, our calculated thermal expansivity at 1 bar pressure, plotted in Figure 10 of our previous work, is too small in the temperature range between 300 K and 500 K compared to the experimental data and the ab initio prediction of Li et al. (2007). In an alternative analysis we represented thermal expansivity predicted by Li et al. (2007) by introducing dispersion in the Grüneisen parameters. We included these results in Table 2 and Table 3. In that case our calculations prefer 1-bar volume data measured by Kajiyoshi et al. (1986). Relative to the description without dispersion these data are only slightly better described, by 0.04% compared to 0.09%, whereas other thermodynamic properties are insignificantly affected. Because the effect of dispersion is small for forsterite, we kept the final result as simple as possible and described it without dispersion in the Grüneisen parameters. The recent data of Trots et al. (2012) could not be represented well. These data require 1-bar thermal expansivity larger than indicated by other data sets in the temperature range between 300 K and 700 K, resulting in a description of 1-bar adiabatic bulk modulus outside the experimental uncertainty in that temperature range.

Contrasted to forsterite the 1-bar volume data of Trots et al. (2012) for the anhydrous form of wadsleyite are preferred by our description. These data appear to be consistent with thermal

expansivity predicted by Wu and Wentzcovitch (2007) and Yu et al. (2013) between 0 and 2000 K and 0 and 20 GPa. Our description is further constrained by adiabatic bulk modulus data measured by Li et al. (1998), which are consistent with new volume-pressure data of the anhydrous form of wadsleyite at ambient temperature measured by Holl et al. (2008).
For the anhydrous form of ringwoodite we used thermal expansivity predicted by Yu et al. (2006) at 1 bar and 21 GPa, which appear to be consistent with volumes measured at 1 bar pressure by Inoue et al. (2004). The upper-left frame of Figure 4 demonstrates that the resulting description is consistent with volume measurements of Katsura et al. (2004). These measurements are based on the MgO pressure scale of Matsui et al. (2000), which in the pressure-temperature range of the measurements, are consistent with the pressure scale of Dorogokupets and Oganov (2007) that we used for all substances. Figure 4 shows that our description represents better these *V-P-T* measurements than the Debye model of Stixrude and Lithgow-Bertelloni (2011). Figure 4 and Figure 3 illustrate that our method allows a more accurate description of volume and entropy of the individual phases, which puts tighter constraints on the Clapeyron slope between wadsleyite and ringwoodite relative to the Debye method. The problem of constraining the Clapeyron slope is more extreme in the database of Fabrichnaya et al. (2004), which represents well the older heat capacity datasets of Ashida et al. (1988) and Watanabe (1982) for both wadsleyite and ringwoodite. Because the parameterization techniques used in this database lack the ability to point to inconsistencies in heat capacity datasets, such as in our method, entropy mismatches that resulting from the more recent heat capacity measurements. Because their Clapeyron slope is not significantly different from our own calculated slope, it is evident that volume for ringwoodite calculated from their database differs from the data of Katsura et al. (2004). That is indeed the case and the deviation appears to be about 1.2% at conditions of the phase transition between wadsleyite and ringwoodite.
In Table 4 we show that thermodynamic properties of forsterite, wadsleyite and ringwoodite are additionally constrained by calorimetric data of Akaogi et al. (2007) and Akaogi et al. (1989), who measured enthalpy differences between them at 1 bar pressure. Because these measurements were carried out at two different temperatures, 298 K and 975 K, they not only put tight restrictions on Clapeyron slopes but also the location of phase boundaries between these phases. Taking additionally into account these measurements, the Clapeyron slope of the wadsleyite-ringwoodite boundary is restricted to values between 5.58 MPa/K and 6.69 MPa/K. That locates the phase boundary between that measured by Katsura et al. (1989) and that of Suzuki et al. (2000), depicted in Figure 1. In the same way the Clapeyron slope of the phase boundary between forsterite and wadsleyite is confined between 1.94 MPa/K and 2.33 MPa/K. Table 4 shows that representing the VDoS of the three polymorphs by a Debye model results in a less accurate representation of the enthalpy difference data of Akaogi et al. (1989, 2007). That is not surprising because Figure 2 indicates that heat capacities and therefore entropies and enthalpies are difficult to represent with this method.

Perovskite, stishovite and periclase

We constrained thermal expansivity and volume of perovskite by measurements of Katsura et al. (2009) depicted in the upper-right frame of Figure 4. That results in a description representing bulk modulus data of Murakami et al. (2007) between 8 GPa and 96 GPa at 300 K to within experimental uncertainty. The resulting bulk modulus is also consistent with ab initio predictions of Tsuchiya et al. (2004) up to 120 GPa. Heat capacity, shown in "online resource, Figure 2", is consistent with the calculations of Chopelas (1996) who applied Kieffer's (1979) model to her Raman spectroscopic measurements.
"Online resource Table 2" shows for stishovite that *V-P-T* measurements are based on several pressure scales. To find a consistent description we directed our analysis towards

measurements based on the Ruby scale, labelled DO7 in "online resource Table 2", because these datasets are in good agreement with each other. Figure 4 and "online resource Table 2" show that these data are also in accordance with data based on other pressures scales, those of Liu et al. (1999) based on NaCl, and those of Andrault et al. (2003) based on quartz. From our analysis it follows that all these data disagree with measurements of Andrault et al. (2003) between 11 GPa and 47 GPa for which pressures were determined using the NaCl scale. They also disagree with those of Panero et al. (2003) whoh used a combination of pressure scales. Our resulting adiabatic bulk modulus at ambient conditions is 301.7 GPa, in accordance with the value 305±5 GPa obtained by Li et al. (1996) by ultrasonic interferometry. Our calculated value for static bulk modulus at zero pressure and zero temperature, 319 GPa, agrees well with that predicted by Oganov et al. (2005), 318 GPa. Our calculated value for the pressure derivative of bulk modulus at ambient conditions is 4.27. This value is difficult to compare with experimental values, because of considerable scatter in them as shown by Li et al. (1996), between 0.7 and 7. For pressures above 47 GPa, at which the $CaCl_2$ form of SiO_2 becomes stable, we used *V-P* data of Andrault et al. (2003) which are based on the platinum scale of Holmes et al. (1989). We converted these pressures to the platinum scale of Dorogokupets and Oganov (2007). To incorporate this form of SiO_2 we used ab initio predictions of Oganov et al. (2005) combined with the Landau formalism, resulting in a transition pressure of 46 GPa at 300 K. Their predicted phase boundary between this form and stishovite is consistent with shockwave measurements of Akin and Ahrens (2002), and we kept it fixed in our calculations, via the model parameters in eqn. (19). Only one fitting parameter, a_L, in eqn. (20) was used to represent volume data. Due to the use of a single pressure scale the effect of the landau contribution to volume is small, only 0.006% at pressures between 80 GPa and 120 GPa, That is much smaller than found by Andrault et al. (2003), between 0.14% and 0.33% in this pressure range.

We used the VDoS and static values for bulk modulus and its pressure derivative predicted by Oganov et al. (2005) to describe columbite, the α-PbO_2 form of SiO_2. We represented their phase boundary to within 0.25 GPa. At 300 K, the transition pressure is 83 GPa, indicating the transformation has gone unnoticed in the measurements of Andrault et al. (2003) presumebly due to kinetic hindrance.

The upper-right frame of "online resource Figure 1" shows for MgO that thermal expansivity at 1 bar pressure calculated using the quasi-harmonic approximation deviates substantially from experimental data measured by Dubrovinsky and Saxena (1997). Compared to the other substances in the system MgO-SiO_2, MgO is unique in the sense that the only way for us to bring agreement in data at 1 bar pressure and shockwave data is to incorporate intrinsic anharmonicity, which additionally must depend on volume. This idea is not new, but has been formulated already by Wu et al. (2008) who used a semi-empirical expression to take into account intrinsic anharmonic effects in the lattice vibrations, thereby expanding the temperature range for which ab initio calculations produces accurate predictions. That intrinsic anharmonicity is present in the lattice vibrations can also be deduced empirically, by calculating the isochoric heat capacity from the numerous data available at 1 bar pressure, such as has been done in Figure 6 of Jacobs and Oonk (2000) up to 1800 K. From that exercise it can be made visible that isochoric heat capacity converges to a value about 4% below the 6R duLong-Petit limit at high temperature, indicating a positive anharmonicity parameter. In the analysis of thermodynamic data we found that shockwave data of Svendsen and Ahrens (1993), up to 200 GPa and shown in "online resource Figure 1", are excellently represented when use is made of the bulk modulus data of Li et al. (2006) who developed a primary pressure scale for MgO using ultrasonic interferometry at room temperature and pressures between 0 and 11 GPa. "Online resource Table 2" shows that our calculations represent their room temperature isotherm, extrapolated to 150 GPa using their pressure scale, with an uncertainty less than 0.05% in volume. This isotherm is also represented well by ab

initio predictions of Wu et al. (2008) in the same pressure range with comparable accuracy. Our results also represent well *V-P-T* data of Kono et al. (2010) who developed a primary pressure scale for MgO using simultaneous measurements of volume and sound wave velocities in the pressure range between 0 and 24 GPa and temperatures between 300 K and 1650 K. "Online resource Figure 1" shows that incorporation of intrinsic anharmonicity in our description results in accurate heat capacity values. "Online resource Table 2" shows that this is also the case for adiabatic bulk modulus.
Taking uncertainties into account for thermodynamic measurements of ringwoodite, MgO and perovskite the uncertainty in the Clapeyron slope of the post-spinel phase boundary shown in Figure 1 is about 0.25 MPa/K. This boundary is slightly curved and its slope decreases from -2.38±0.25 MPa/K at 2143 K to -1.82±0.25 MPa/K at 1300 K. The triple point in which wadsleyite, ringwoodite, perovskite and MgO are in equilibrium is constrained to 2160±50 K, 22.5±0.5 GPa.

Akimotoite, majorite and post-perovskite

Contrary to the analysis of Jacobs and de Jong (2007), we constrained thermal expansivity of akimotoite between 0 and 2000 K, and 0 and 30 GPa with that predicted by Karki and Wentzcovitch (2002). That results in an accurate description of the 1-bar volume data of Horiuchi (1982) and Ashida et al. (1988) up to 1000 K. To establish an accurate description for bulk modulus we used the room temperature *V-P* data of Reynard et al. (1996a) and *V-P-T* data of Wang et al. (2004). Pressures in the first dataset are based on the ruby scale of Mao et al. (1986), whereas those of the last dataset are based on the gold scale of Anderson (1989). Pressures in these datasets were converted to pressures based on the scale of Dorogokupets and Oganov (2007) and the results are shown in "online resource Figure 3". Our calculated bulk modulus at ambient conditions is consistent with the value 212 GPa measured ultrasonically by Ito and Weidner (1985). The phase boundary between akimotoite and perovskite is constrained by the combined datasets of Hirose et al. (2001) and Ono et al. (2001), as published by Fei et al. (2004) based on the MgO scale of Speziale et al. (2001). We converted pressures from that scale to that of Dorogokupets and Oganov (2007), leading to small corrections for pressure less than 0.4 GPa. To represent the Clapeyron slope we introduced a value of -1.2×10^{-5} K^{-1} for the intrinsic anharmonicity parameter for akimotoite, consistent with the value $-(0.9\pm0.7)\times10^{-5}$ K^{-1} determined by Reynard et al. (1996b) using Raman spectroscopy. We arrived at a value of -3.8±0.27 MPa/K for the Clapeyron slope. Due to anharmonicity in the lattice vibrations of akimotoite, the Clapeyron slope of the phase boundary between wadsleyite+stishovite and akimotoite is small, -0.33±0.28 MPa/K. Figure 2 shows that its location and slope agrees well with the measured phase diagram data of Ito and Navrotsky (1985) and Sawamoto (1987).
Thermal expansivity in *P-T* space of majorite is tightly constrained by predictions of Yu et al. (2011), illustrated in the upper-left frame of Figure 5. Representing the steep behaviour of thermal expansivity at low temperatures and its flat behaviour above 500 K, required dispersion in Grüneisen parameters, for which we used the Raman spectroscopic data of Chopelas (2000). Using her data, a simple description was achieved by averaging Grüneisen parameters in two frequency ranges. Figure 2 shows that Sawamoto's (1987) phase field is represented quite well by the calculations. Above about 20 GPa and 2300 K Chudinovskikh and Boehler (2004) found perovskite as the stable phase instead of majorite, indicating pressure calibration problems in Sawamoto's (1987) experiments at these conditions.
For post-perovskite the *V-P-T* measurements of Guignot et al. (2007), plotted in Figure 5, are represented insignificantly different compared to the description of Jacobs and de Jong (2007). These measurements are based on the MgO pressure scale of Karki et al. (2000), for which pressures deviate less than 0.7 GPa from those resulting from the MgO scale by Dorogokupets

and Oganov (2007). Additionally we constrained thermal expansivity by the macroscopic Grüneisen parameter predicted by Tsuchiya et al. (2005) in the temperature range between 0 and 4000 K and pressure range between 0 and 150 GPa. Our calculated bulk modulus represents well that predicted by Tsuchiya et al. (2005) and Oganov et al. (2002) in this *P-T* range. We find a value of 9.8±2.7 MPa/K for the Clapeyron slope of the phase boundary between perovskite and post-perovskite.

Orthoenstatite, HPclinoenstatite, LPclinoenstatite

We fine-tuned our description for orthoenstatite in Jacobs et al. (2013) by using a 4th order Birch-Murnaghan equation of state for the static lattice to represent the curvature in the bulk modulus data depicted in Figure 5. This fine-tuning was also necessary to represent the equilibrium between the Low-pressure clinoenstatite and orthoenstatite, which is characterized by small entropy differences of about 0.7 JK^{-1}mol^{-1} and volume differences of about 0.06 cm^3/mol. Thermodynamic properties of Low-pressure clinoenstatite are tightly constrained by accurate low-temperature heat capacity data, *V-T* data at 1 bar up to 1100 K and *V-P* data at 300 K up to 7 GPa, resulting in a description representing well ab initio predictions of thermal expansivity by Yu et al. (2010). For High-pressure clinoenstatite we found a description insignificantly different from that of Jacobs and de Jong (2007). An overview of experimental data for phase equilibria between the three polymorphs is given by Ulmer and Stalder (2001), indicating significant uncertainties in the locations of phase boundaries between these three phases. We constrained the location of the boundary between orthoenstatite and HPclinoenstatite by experimental data of Pacalo and Gasparik (1990) because the steeper boundary suggested by Ulmer and Stalder (2001) results in a too flat phase boundary between HPclinoenstatite and wadsleyite+stishovite, and a phase boundary between HPclinoenstatite and majorite having a too negative Clapeyron slope. For the construction of the phase boundaries between LPclinoenstatite and orthoenstatite and between LPclinoenstatite and HPclinoenstatite we followed the work of Angel et al. (1994), resulting in a triple point of 7.88 GPa and 1184 K, consistent with their location of 7.9 GPa, 1173 K, but deviating from the value given by Ulmer and Stalder (2001), 6.6 GPa and 1093 K.

Shear modulus

Descriptions for shear modulus were obtained by fitting parameters b_ν in eqn. (5) and $n_{s,0}$ in eqn. (14) after the analysis of thermodynamic data was carried out. From the analyses it was found that shear modulus data do not put tighter constraints on the thermodynamic description. "Online resource Table 2" shows that for most polymorphs sufficient experimental data are available and our optimization resulted in a representation of these data insignificantly different from that obtained by Jacobs and de Jong (2007). Examples are given in Figure 5 for orthoenstatite and high-pressure clinoenstatite. For a number of polymorphs no or few experimental data are available, which we discuss here. For low-pressure clinoenstatite no experimental shear modulus data are available. We estimated the value for the static shear modulus, $G_0^{st,lcen}$ by relating this property to bulk modulus and by taking the same Poisson ratio, ν, as for orthoenstatite, by making use of the well-known relation:

$$G_0^{st,lcen} = \frac{3(1-2\nu)}{2(1+\nu)} K_0^{st,lcen} \qquad (1)$$

Other static parameters related to the pressure derivative of shear modulus and the vibrational contributions to shear modulus were assumed to be identical with that for orthoenstatite. For

majorite also no experimental data are available, and we constrained the model parameters by extrapolating between experimental data for pyrope and a mixture of 50% pyrope and 50% majorite, measured by Gwanmesia et al. (2000, 2009).
For a number of polymorphs only experimental data at ambient conditions are available, such as for akimotoite. For akimotoite we constrained pressure and temperature derivatives by ab initio calculations of Karki et al. (2001) and Li et al. (2009). For perovskite and post-perovskite we constrained temperature derivatives of shear modulus by ab initio data, given in "online resource Table 2", with the additional constraint that longitudinal, bulk and shear sound velocity contrast at the perovskite-postperovskite phase boundary represent ab initio calculations by Wentzcovitch et al. (2006). Our model description for the transformation of stishovite to the $CaCl_2$ form of SiO_2 is incomplete, because no Landau contribution has been incorporated in the shear modulus, only in thermodynamic properties. We constrained shear modulus and its pressure derivative at 300 K by experimental data of Li et al. (2009) between 0 and 3 GPa, which appear to be consistent with recent ab initio predictions of Yang et al. (2014). Because of the incompleteness of our model, we mismatch shear modulus predicted by ab initio in the pressure range between 20 GPa and 60 GPa. For most applications of our database to earth materials this is not problematic because stishovite does not appear in phase assemblages above about 25 GPa, also not when FeO is added to the MgO-SiO_2 system.

R**eferences**

Akaogi M, Yusa H, Shiraishi K, Suzuki T (1995) thermodynamic properties of α-quartz, coesite, and stishovite and equilibrium phase relations at high pressures and high temperatures, J Geophys Res 100:22337-22347

Akaogi M, Oohata M, Kojitani H, Kawaji H (2011) Thermodynamic properties of stishovite by low-temperature heat capacity measurements and the coesite-stishovite transition boundary. Am Mineral 96:1325-1330

Anderson OL, Isaak DG, Yamamoto S (1989) Anharmonicity and the equation of state for gold. J Appl Phys 65:1534-1543

Angel RJ, Finger LW, Hazen RM, Kanzaki M, Weidner DJ, Liebermann RC, and Veblen DR (1989), Structure and twinning of single-crystal $MgSiO_3$ garnet synthesized at 17 GPa and 1800 °C. Am Mineral 74:509-512

Barin I (1989) Thermochemical Data of Pure Substances, Part II, VCH Verlags-gesellschaft mbH, D6940 Weinheim (FRG)

Barron THK, Berg WT, Morrison JA (1959) On the heat capacity of crystalline magnesium oxide. Proc Roy Soc (London) 250A:70

Bosenick A, Geiger CA, Cemič L (1996) Heat capacity measurements of synthetic pyrope-grossular garnets between 320 and 1000 K by differential scanning calorimetry. Geochim Cosmochim Acta 60:3215-3227

Bouhifd MA, Andrault D, Fiquet G, Richet P (1996) Thermal expansion of forsterite up to the melting point. Geophys Res Lett 23:1143-1146

Brazhkin VV, McNeil LE, Grimsditch M, Bendeliani NA, Dyuzheva TI, Lityagina LM (2005) Elastic constants of stishovite up to its amorphization temperature. J Phys Condens Mater 17:1869-1875

Chase Jr MW, Davies CA, Downey Jr JR, Frurip DJ, McDonald RA, Syverud AN (1985) J Phys Chem Ref Data Suppl 1(14), p1469

Chopelas A (1996) Thermal expansivity of lower mantle phases MgO and $MgSiO_3$ perovskite at high pressure derived from vibrational spectroscopy. Phys Earth Planet Int 98:3-15

Dachs E, Geiger CA, Seckendorff von V, Grodzicki M (2007) A low-temperature calorimetric study of synthetic (forsterite + fayalite) $\{Mg_2SiO_4 + Fe_2SiO_4\}$ solid solutions: An analysis of vibrational, magnetic, and electronic contributions to the molar heat capacity and entropy of mixing. J Chem Thermodynamics 39:906-933

Deon F, Koch-Müller M, Rhede D, Gottschalk M, Wirth R, Thomas SM (2010) location and quantification of hydroxyl in wadsleyite: New insights. Am Mineral 95:312-322

Downs RT, Zha C-S, Duffy TS, Finger LW (1996) The equation of state of forsterite to 17.2 GPa and effects of pressure media. Am Mineral 81:51-55

Dubrovinsky LS, Saxena SK (1997) Thermal expansion of periclase (MgO) and Tungsten (W) to melting temperatures. Phys Chem Minerals 24:547-550

Duffy TS, Ahrens TJ (1995) Compressional sound velocity, equation of state, and constitutive response of shock-compressed magnesium oxide. J Geohys Res B 100:529-542

Fatyanov OV, Asimow PD, Ahrens TJ (2009) Shock temperatures of preheated MgO. In: Shock Compression of Condensed Matter, M.L. Elert, W.T. Buttler, M.D. Furnish, W.W. Anderson, W.G. Proud, eds), pp 855-858

Fei Y (1999) Effects of temperature and composition on the bulk modulus of (Mg,Fe)O. Am Mineral 84:272-276

Fiquet G, Andrault D, Dewaele A, Charpin T, Kunz M, Haüsermann D (1998) *P-V-T* equation of state of $MgSiO_3$ perovskite. Phys Earth Plan Inter 105:21-31.

Fiquet G, Richet P, Montagnac G (1999) High-temperature thermal expansion of lime, periclase, corundum and spinel. Phys Chem Minerals 27:103-111

Funamori N, Yagi T, Utsumi W, Kondo T, Uchida T, Funamori M (1996) Thermoelastic properties of $MgSiO_3$ perovskite determined by in situ X-ray observations up to 30 GPa

and 2000 K. J Geophys Res 101:8257-8269.
Gwanmesia GD, Rigden S, Jackson I, Liebermann RC (1990) Pressure dependence of elastic wave velocity for β-Mg_2SiO_4 and the composition of the Earth's mantle. Science 250:794-797
Gwanmesia GD, Liu J, Chen G, Kesson S, Rigden SM, Liebermann RC (2000) Elasticity of the pyrope ($Mg_3Al_2Si_3O_{12}$).majorite ($MgSiO_3$) garnets solid solution. Phys Chem Minerals 27:445-452
Gwanmesia GD, Wang L, Triplett R, Liebermann RC (2009) Pressure and temperature dependence of the elasticity of pyrope-majorite [$Py_{60}Mj_{40}$ and $Py_{50}Mj_{50}$] garnets solid solution measured by ultrasonic interferometry technique. Pys Earth Plan Int 174:105-112
Hazen RM, Zhang J, Ko J (1990) Effects of Fe/Mg on the compressibility of synthetic wadsleyite: β-$(Mg_{1-x}Fe_x)_2SiO_4$ ($x \leq 0.25$). Phys Chem Minerals 17:416-419
Hazen RM, Weinberger MB, Yang H, Prewitt CT (2000) Comparative high-pressure crystal chemistry of wadsleyite, β-$(Mg_{1-x}Fe_x)_2SiO_4$ with x=0 and 0.25. Am Mineral 85:770-777
Hofmeister AM (1992) Thermodynamic properties of $MgSiO_3$ ilmenite from vibrational spectra. Phys Chem Minerals 18:423-432
Holl CM, Smyth JR, Jacobsen SD, Frost DJ (2008) Effects of hydration on the structure and compressibility of wadsleyite, β-(Mg_2SiO_4). Am Mineral 93:598-607
Horiuchi H, Hirano M, Ito E, Matsui Y (1982) $MgSiO_3$ (ilmenite-type): single crystal X-ray diffraction study. Am Mineral 67:788-793
Horiuchi H, Ito E, Weidner DJ (1987) Perovskite-type $MgSiO_3$: single crystal X-ray diffraction study. Am Mineral 72:357-360
Hugh-Jones D (1997) thermal expansion of $MgSiO_3$ and $FeSiO_3$ ortho- and clinopyroxenes. Am Mineral 82:689-696
Inoue T, Tanimoto Y, Irifune T, Suzuki T, Fukui H, Ohtaka O (2004) Thermal expansion of wadsleyite and hydrous ringwoodite. Phys Earth Plan Int 143-144:279-290
Isaak DG, Anderson OL, Goto T (1989) Elasticity of single-crystal forsterite measured to 1700 K. J Geophys Res 94:5895-5906
Isaak DG, Anderson OL, Goto T (1989) Measured elastic moduli of single-crystal MgO up to 1800 K. Phys Chem Minerals 16:704-713
Ito E, Matsui Y (1978) Synthesis and crystal chemical characterization of $MgSiO_3$ perovskite. Earth Planet Sci Lett 38:443-450
Jackson JM, Sinogeikin SV, Bass JD (2000) Sound velocities and elastic properties of γ-Mg_2SiO_4 to 873 K by Brillouin spectroscopy. Am Mineral 85:296-303
Jackson JM, Palko JW, Andrault D, Sinogeikin SV, Lakshtanov DL, Wang J, Bass JD, Zha C-S (2003) Thermal expansion of natural orthoenstatite to 1473 K. Eur J Mineral 15:469-473
Jackson JM, Sinogeikin SV, Bass JD (2007) Sound velocities and single-crystal elasticity of orthoenstatite to 1073 K at ambient pressure. Phys Earth Plan Int 161:1-12
Jacobs MHG, Oonk HAJ (2000) A realistic equation of state for solids. The high pressure and high temperature thermodynamic properties of MgO. Calphad 24:133-147
Jacobsen SD, Holl CM, Adams KA, Fischer RA, Martin ES, Bina CR, Lin J-F, Prakapenka VB, Kubo A, Dera P (2008) Compression of single-crystal magnesium oxide to 118 GPa and a ruby pressure gauge for helium pressure media. Am Mineral 93:1923-1828
Jiang F, Gwanmesia GD, Dyuzheva T, Duffy TS (2009) Elasticity of stishovite and acoustic mode softening under high pressure by Brillouin scattering. Phys Earth Plan Int 172:235-240
Karki BB, Wentzcovitch RM, de Gironcoli S, Baroni S (2000a) Ab initio lattice dynamics of $MgSiO_3$ perovskite at high pressure. Phys Rev B 62:14750-14756
Karki BB, Wentzcovitch RM, de Gironcoli S, Baroni S (2000b) High-pressure lattice

dynamics and thermoelasticity of MgO. Phys Rev B 61:8793-8800
Karki BB, Wentzcovitch RM (2002) First-principles lattice dynamics and thermoelasticity of $MgSiO_3$ ilmenite at high pressure. J Geophys Res 107:2267
Kato T, Kumazawa M (1985) Garnet phase of $MgSiO_3$ filling the pyroxene-ilmenite gap at very high temperature. Nature 316:803-805.
Krupka KM, Robie RA, Hemingway BS (1979) High-temperature heat capacities of corundum, periclase, anorthite, $CaAl_2Si_2O_8$ glass, muscovite, pyrophyllite, $KALSi_3O_8$ glass, grossular, and $NaAlSi_3O_8$ glas. Am Mineral 64:86-101
Kudoh Y, Ito E, Takeda H (1987) Effect of pressure on the crystal structure of perovskite-type $MgSiO_3$. Phys Chem Minerals 14:350-354
Kung J, Li B (2014) Lattice dynamic behavior of orthoferrosilite ($FeSiO_3$) toward phase transition and compression. J Phys Chem C, 118, 12410-12419
Li B, Gwanmesia GD, Liebermann RC (1996) Sound velocities of olivine and beta polymorphs of Mg_2SiO_4 at Earth's transition zone pressures. Geophys Res Lett 23:2259-2262
Li B, Rigden SM, Liebermann RC (1996) Elasticity of stishovite at high pressure. Phys Earth Plan Int 96:113-127
Li B, Liebermann, Weidner DJ (1998) Elastic moduli of wadsleyite (β-Mg_2SiO_4) to 7 Gigapascals and 873 Kelvin. Science 281:675-677
Li B (2003) Compressional and shear wave velocities of ringwoodite γ-Mg_2SiO_4 to 12 GPa. Am Mineral 88:1312-1317
Li L, Weidner DJ, Brodholt J, Alfè, Price G (2009) Ab initio molecular dynamics study of elasticity of akimotoite $MgSiO_3$ at mantle conditions. Phys Earth Plan Int 173:115-120
Lu R, Hofmeister AM, Wang YB (1994) Thermodynamic properties of ferromagnesium silicate perovskites from vibrational spectroscopy. J Geophys Res B, 99:11795-11804
Marsh SP (1980) LASL shock Hugoniot data. University of California Press, Berkeley
Matsubara R, Toraya H, Tanaka S, Sawamoto H (1990) Precision lattice parameter determination of $(Mg,Fe)SiO_3$ tetragonal garnets. Science 247:697-699.
Matsui T, Manghnani MH (1985) Thermal expansion of single-crystal forsterite to 1023 K by Fizeau Interferometry. Phys Chem Minerals 12:201-210
Meng Y, Weidner DJ, Gwanmesia GD, Liebbermann RC, Vaughan MT, Wang Y, Leinenweber K, Pacalo RE, Yeganeh-Haeri A, Zhao Y (1993) In situ high P-T X ray diffraction stdies on three polymorphs (α,β,γ) of Mg_2SiO_4. J Geophys Res 98:22199-22207
Ming LC, Manghnani MH, Kim YH, Usha-Devi S, Xu JA, Ito E (1992) Thermal expansion studies of $(Mg,Fe)_2SiO_4$-spinels using synchrotron radiation. In: Advances in Physical Geochemistry (ed. S Saxena), pp 315-334. Springer-Verlag, New York
Mraw SC, Naas DF (1979) the measurement of accurate heat capacities by differential scanning calorimetry. Comparison of d.s.c. results on pyrite (100 to 800 K) with literature values from precision adiabatic calorimetry. J Chem Thermodyn 11:567-584
Murakami M, Sinogeikin SV, Hellwig H, Bass JD, Li J (2007) Sound velocity of $MgSiO_3$ perovskite to Mbar pressure. Earth Plan Sci Lett 256:47-54
Oganov AR, Dorogokupets PI (2003) All-electron and pseudopotential study of MgO: equation of state, anharmonicity, and stability. Phys Rev B 67:224110,1-11
Oganov AR, Ono S (2004) Theoretical and experimental evidence for a post-perovskite phase of $MgSiO_3$ in Earth's D'' layer. Nature 430:445-448
Ono S, Kikegawa T, Ohishi Y (2006) Equation of state of $CaIrO_3$-type $MgSiO_3$ up to 144 GPa. Am Mineral 91:475-478.
Pacalo REG, Weidner D.J. (1997) Elasticity of majorite, $MgSiO_3$ tetragonal garnet. Phys Earth Planet Int, 99:145-154.
Peteghem CB van, Zhao J, Angel RJ, Ross NL, Bolfan-Casanova N. (2006) Crystal structure

and equation of state of $MgSiO_3$ perovskite. Geophys Res Lett, 33: L03306, doi: 10.1029/2005GL024955
Reynard B, Fiquet G, Itié, Rubie DC (1996a) High-pressure X-ray diffraction study and equation of state of $MgSiO_3$ ilmenite. Am Mineral 81:45-50
Richet P, Fiquet G (1991) High-temperature hear capacity and premelting of minerals in the system MgO-CaO-Al_2O_3-SiO_2. J Geophys Res 96:445
Ross NL, Hazen RM (1989) Single-crystal X-ray diffraction study of $MgSiO_3$ perovskite from 77 to 400 K. Phys Chem Minerals 16:415-420
Ross NL, Hazen RM (1990) High-pressure crystal chemistry of $MgSiO_3$ perovskite. Phys Chem Minerals 17:228-237
Saxena SK, Dubrovinsky LS, Tutti F, Le Bihan T (1999) Equation of state of $MgSiO_3$ with the perovskite structure based on experimental measurements. Am Mineral 84:226-232
Shinmei T, Tomioko N, Fujino K, Kuroda K, Irifune T (1999) In situ X-ray diffraction study of enstatite up to 12 GPa and 1473 K and equation of state. Am Mineral 84:1588-1594
Sinogeikin SV, Bass JD, O'Neill B, Gasparik T (1997) Elasticity of tetragonal end-member majorite and solid solutions in the system $Mg_4Si_4O_{12}$-$Mg_3Al_2Si_3O_{12}$. Phys Chem Minerals 24:115-121
Sinogeikin SV, Bass JD (1999) Single-crystal elasticity of MgO at high pressure. Phys Rev B 59:R14141-R14144
Sinogeikin SV, Jackson JM, O'Neill B, Palko JM, Bass JD (2000) Compact high-temperature cell for Brillouin scattering measurements. Rev Sci Instr 71:201-206
Sinogeikin SV, Bass JD, Katsura T (2003) Single-crystal elasticity of ringwoodite to high pressures and high temperatures: implications for 520 km seismic discontinuity. Phys Earth Plan Int 136:41-66
Sinogeikin SV, Zhang J, Bass JD (2004) Elasticity of single crystal and polycrystalline $MgSiO_3$ perovskite by Brillouin spectroscopy. Geophys Res Lett 31:L06620, doi 10.1029/2004GL019559
Sugahara M, Yoshiasa A, Komatsu Y, Yamanaka T, Bolfan-Casanova N, Nakatsuka A, Sasaki S., and Tanaka M. (2006) Reinvestigation of the $MgSiO_3$ perovskite structure at high pressure. Am Mineral, 91:533-536.
Sumino Y, Nishizawa O, Goto T, Ozima M (1977) Temperature variation of elastic constants of single-crystal forsterite between -190 and 400 °C. J Phys Earth 25:377-392
Sumino Y, Anderson OL, Suyuki I (1983) Temperature coefficients of elastic constants of single-crystal MgO between 80 and 1300 K. Phys Chem Minerals 9:38-47
Suzuki I (1979) Thermal expansion of γ-Mg_2SiO_4. J Phys Earth 27:53-61
Suzuki I (1980) Thermal expansion of modified spinel, β-Mg_2SiO_4. J Phys Earth 28:273-280
Suzuki I, Anderson OL, Sumino Y (1983) Elastic properties of a single-crystal forsterite Mg_2SiO_4 up to 1200 K. Phys Chem Minerals 10:38-46
Suzuki I, Takei H, Anderson OL (1984) Thermal expansion of single-crystal forsterite, Mg_2SiO_4. Proceedings of the 8th Int Thermal Expansion Symposium, sponsored by the National Bureau of Standards, Plenum Publ. Co, New York, pp 79-88
Trots DM, Kurnosov A, Ballaran TB, Frost DJ (2012) High-temperature structural behaviors of anhydrous wadsleyite and forsterite. Am Mineral 97:1582-1590
Tsuchiya T, Tsuchiya J, Umemoto K, Wentzcovitch RM (2004) Elasticity of post-perovskite $MgSiO_3$. Geophys Res Lett 21:L14603
Ulmer P, Stalder R (2001) The $Mg(Fe)SiO_3$ orthoenstatite-clinoenstatite transitions at high pressures and temperatures determined by Raman-spectroscopy on quenched samples. Am Mineral 86:1267-1274
Utsumi W, Funamori N, and Yagi T (1995), Thermal expansivity of $MgSiO_3$ perovskite under high pressures up to 20 GPa. Geophys Res Lett 22:1005-1008.
Victor AC, Douglas TB (1963) Thermodynamic properties of magnesium oxide and

beryllium oxide from 298 to 1200 ºK. J Research of the Natl Bureau of Standards – A, Physics and Chemistry. 67A:325-329
Wang Y, Weidner DJ, Liebermann RC, Zhao Y (1994) PVT equation of state of (Mg,Fe)SiO_3 perovskite: constraints on composition of the lower mantle. Phys Earth Plan Inte 83:13-40
Wang Y, Uchida T, Zhang J, Rivers ML, Sutton SR (2004) Thermal equation of state of akimotoite $MgSiO_3$ and effects of the akimotoite-garnet transformation on seismic structure near the 660 km discontinuity. Phys Earth Planet Int, 143-144:57-80
Weidner DJ, Bass JD, Ringwood AE, Sinclair W (1982) The single-crystal elastic moduli of stishovite. J Geophys Res B 87:4740-4746
Weidner DJ, Ito E (1985) Elasticity in the ilmenite phase. Phys Earth Plan Int 40:65-70
Wentzcovitch RM, Tsuchiya T, Tsuchiya J (2006) $MgSiO_3$ postperovskite at D'' conditions. Proc Natl Am Soc 103:543-546
Wu Z, Wentzcovitch RM (2007) Vibrational and thermodynamic properties of wadsleyite: A density functional study. J Geophys Res 112:B12202, 1-11
Wu Z, Justo JF, da Silva CRS, de Gironcoli S, Wentzcovitch RM (2009) Anomalous thermodynamic properties in ferropericlase throughout its spin crossover. Phys Rev B 80:014409, 1-8
Yagi T, Uchiyama Y, Akaogi M, Ito E (1992) Isothermal compression curve of $MgSiO_3$ tetragonal garnet. Phys Earth Plan Int 74:1-7
Yamanaka T Fukuda T, Tsuchiya J (2002) Bonding character of SiO_2 stishovite under high pressures up to 30 GPa. Phys Chem Minerals 29:633-641
Yang H, Ghose S (1995) High temperature single crystal X-ray diffraction studies of the ortho-proto phase transition in enstatite, $Mg_2Si_2O_6$ at 1360 K. Phys Chem Minerals 22:300-310
Yang R, Wu Z (2014) Elastic properties of stishovite and the $CaCl_2$-type silica at the mantle temperature and pressure: an ab initio investigation. Earth Plan Sci Lett 404:14-21
Ye Y, Schwering RA, Smyth JR (2009) Effects of hydration on thermal expansion of forsterite, wadsleyite, and ringwoodite at ambient pressure. Am Mineral 94:899-904
Yeganeh-Haeri A (1994) Synthesis and re-investigation of the elastic properties of single-crystal magnesium silicate perovskite. Phys Earth Plan Inter, 87:111-112.
Yong W, Dachs E, Benisek A, Secco RA (2012) Heat capacity, entropy and phase equilibria of stishovite. Phys Chem Minerals 39:153-162
Yu YG, Wentzcovitch RM (2006) Density functional study of vibrational and thermodynamic properties of ringwoodite. J Geophys Res 111:B12202, 1-8
Yu YG, Wentzcovitch RM, Angel RJ (2010) First principles study of thermodynamics and phase transition in low-pressure ($P2_1/c$) and high-pressure ($C2/c$) clinoenstatite $MgSiO_3$). J Geophys Res 115:B02201
Zha C-S, Duffy TS, Downs RT, Mao H-K, Hemley RJ (1996) Sound velocity and elasticity of single-crystal forsterite to 16 GPa. J Geophys Res 101:17535-17545
Zha C-S, Duffy TS, Mao H-k, Downs RT, Hemley RJ, Weidner DJ (1997) Single-crystal elasticity of β-Mg_2SiO_4 to the pressure of the 410 km seismic discontinuity in the Earth's mantle. Earth Plan Sci Lett 147:E9-E15
Zha C-S, Mao H-k, Hemley RJ (2000) Elasticity of MgO and a primary pressure scale to 55 GPa. Proc Natl Acad Sci of the USA 97:13494-13499
Zhang L (1998) Single crystal hydrostatic compression of $(Mg,Mn,Fe,Co)_2SiO_4$. Phys Chem Minerals 25:308-312

Table 1. Fractions in the VDoS of each substance, multiplied by 100. A 30-Einstein model has been used for each substance

Fo										
1	0.0395	6	5.6118	11	7.1642	16	3.8264	21	0.0422	26	2.5889
2	0.2804	7	5.0486	12	5.1693	17	3.6384	22	0.0094	27	1.9938
3	0.7458	8	6.1179	13	5.6160	18	3.0954	23	0.3478	28	2.1333
4	1.7440	9	7.6923	14	5.9959	19	0.1273	24	4.7549	29	2.9142
5	4.4500	10	7.5042	15	6.2090	20	0.0258	25	4.4462	30	0.6672
Wa										
1	0.0332	6	3.6979	11	8.4537	16	7.0483	21	2.3967	26	3.2419
2	0.1861	7	5.2560	12	7.8133	17	3.7919	22	0.3038	27	4.1833
3	0.4526	8	6.3041	13	6.4169	18	2.6937	23	1.7380	28	1.8135
4	0.9209	9	5.8879	14	5.7955	19	0.9735	24	2.3029	29	0.9532
5	1.6975	10	6.5494	15	5.7122	20	0.4415	25	2.1194	30	0.8211
1	0.0168	6	2.0713	11	4.9434	16	6.5343	21	0.0000	26	6.9389
Ri										
2	0.1401	7	5.3139	12	7.1663	17	4.2876	22	0.0000	27	1.4037
3	0.3372	8	4.1357	13	7.0551	18	4.2411	23	0.0000	28	1.2355
4	0.6500	9	4.9999	14	9.8450	19	5.7650	24	0.3591	29	0.6843
5	1.1461	10	6.5402	15	6.2150	20	0.2639	25	6.2201	30	1.4905
Pc										
1	0.0001	6	0.4777	11	3.4481	16	5.0228	21	4.3243	26	1.8622
2	0.0157	7	0.7385	12	6.0123	17	8.9735	22	1.8180	27	1.4825
3	0.0675	8	1.0960	13	8.3892	18	13.4130	23	3.7999	28	1.1465
4	0.1493	9	1.5720	14	5.2248	19	11.3661	24	3.9899	29	0.8076
5	0.2918	10	2.2926	15	3.6968	20	5.7120	25	2.5619	30	0.2472
St										
1	0.0009	6	0.8041	11	4.4971	16	3.8226	21	6.1284	26	2.6286
2	0.0465	7	1.5676	12	4.0362	17	5.2475	22	4.0951	27	4.1059
3	0.1393	8	2.4465	13	7.6479	18	4.7394	23	3.3442	28	2.7651
4	0.2568	9	4.0875	14	6.5776	19	4.9609	24	4.5493	29	1.3861
5	0.5154	10	5.7606	15	4.3024	20	6.1199	25	2.9906	30	0.4297
St-II										
1	0.0000	6	0.6702	11	4.6267	16	5.3746	21	5.5788	26	3.2591
2	0.0009	7	1.0875	12	4.9974	17	6.2176	22	3.5663	27	3.9168
3	0.0588	8	1.8711	13	5.2213	18	6.4395	23	3.5029	28	2.3054
4	0.2503	9	2.7964	14	5.0882	19	8.4655	24	3.9369	29	1.2377
5	0.4577	10	3.4518	15	6.9625	20	6.5044	25	1.8051	30	0.3484
Pv										
1	0.0096	6	2.2789	11	4.9651	16	5.5576	21	3.7203	26	0.3634
2	0.1033	7	5.0952	12	5.4108	17	6.2691	22	4.3931	27	2.1900
3	0.2033	8	5.5605	13	4.5170	18	5.8823	23	5.7013	28	2.7360
4	0.3431	9	4.8279	14	4.3340	19	5.1884	24	3.6329	29	1.1197
5	0.8542	10	4.5661	15	4.5131	20	4.2907	25	1.1051	30	0.2679
Ppv										
1	0.0000	6	1.2234	11	3.7483	16	5.1006	21	5.5801	26	0.9304
2	0.0032	7	2.0785	12	4.5262	17	5.6265	22	4.8636	27	2.0865
3	0.0508	8	3.7310	13	6.0844	18	5.7873	23	3.8986	28	2.9353
4	0.2373	9	5.7734	14	5.7794	19	5.6824	24	3.1534	29	0.8433
5	0.5992	10	5.6798	15	5.7443	20	6.2245	25	1.9317	30	0.0967

Table 1. (continued)

Aki										
1	0.0000	6	1.9275	11	6.0342	16	7.2053	21	3.1691	26	7.2007
2	0.0160	7	2.8685	12	5.6909	17	6.2926	22	3.8530	27	1.8821
3	0.2207	8	3.7171	13	4.7488	18	3.4391	23	3.2868	28	1.3290
4	0.4689	9	4.0454	14	4.5972	19	4.4495	24	3.2757	29	0.9126
5	0.9638	10	3.9765	15	5.3508	20	4.3016	25	4.5167	30	0.2597
Mj										
1	0.0088	6	5.4356	11	5.4259	16	3.5251	21	0.6871	26	6.0083
2	0.2875	7	6.9618	12	4.8335	17	3.6269	22	0.0143	27	3.2123
3	0.9069	8	7.1291	13	4.3867	18	2.0319	23	0.5422	28	2.6489
4	2.4466	9	6.3865	14	4.4916	19	2.4281	24	2.0107	29	1.2669
5	4.0129	10	6.6567	15	4.6650	20	2.6304	25	3.6102	30	1.7217
HCen										
1	0.0411	6	5.7855	11	7.0029	16	3.3595	21	2.2817	26	1.9301
2	0.3684	7	6.0058	12	5.7413	17	2.7806	22	1.8228	27	2.8552
3	1.1640	8	6.1399	13	5.5476	18	3.9029	23	1.0343	28	1.9430
4	2.8107	9	6.5528	14	4.4031	19	3.4535	24	2.4603	29	0.5632
5	4.4223	10	6.8718	15	3.8597	20	2.4809	25	2.0920	30	0.3232
LCen										
1	0.0606	6	5.5283	11	7.1349	16	1.5051	21	0.0344	26	1.5514
2	0.5467	7	5.5062	12	7.0081	17	0.8499	22	0.7204	27	3.9713
3	1.6474	8	5.9036	13	2.9362	18	2.6399	23	1.0762	28	4.8179
4	3.1875	9	7.9081	14	5.2630	19	2.5367	24	2.6954	29	1.1762
5	4.7732	10	7.7284	15	6.2654	20	1.2599	25	3.3377	30	0.4300
Oen										
1	0.0716	6	5.7491	11	6.0243	16	2.3749	21	2.2956	26	2.8750
2	0.7621	7	6.4253	12	5.2695	17	2.1703	22	1.7757	27	1.9759
3	2.2932	8	6.9805	13	4.2834	18	3.1633	23	1.6909	28	0.6784
4	4.3252	9	6.3718	14	4.3168	19	3.0721	24	3.0083	29	0.5524
5	5.3528	10	6.1987	15	3.8030	20	3.1517	25	2.7076	30	0.2808

VDoS taken from: Fo: Li et al (2007); Wa: Wu & Wentzcovitch (2007); Ri: Yu & Wentzcovitch (2006); Pc: Wu et al (2009); St, St-I,II: Oganov et al (2005); Pv: Karki et al (2000); Ppv: Tsuchiya et al (2005); Aki: Karki & Wentzcovitch (2002); Mj: Yu et al. (2011); Hcen, Oen: Choudhury & Chaplot (2000); Lcen: Yu et al (2010)

Table 2. Representation of experimental thermodynamic properties for polymorphs in the system MgO-SiO_2. DO07 indicates data are based on the pressure scale of Dorogokupets & Oganov (2007). Italicized references are ab initio results.

Property	Max. relative deviation in %	Average relative deviation in %	*T*-range in K	*P*-range in GPa	Reference
Ortho enstatite					
Volume	0.10	0.03	298	0.0-8.5	Angel & Hugh-Jones (1994)
	0.27	0.15	298	0.0-9.6	Kung et al. (2004)
	0.62	0.38	296-1360	0.0	Yang & Ghose (1995)
	0.20	0.08	298-1001	0.0-4.52	Zhao et al. (1995)
	0.28	0.11	293-1094	0.0	Hugh-Jones (1997)
	0.53	0.24	300-1473	0.0	Jackson et al. (2003)
	0.38	0.31	294-1073	0.0	Jackson et al. (2007)
K_S	1.85	0.99	294-1073	0.0	Jackson et al (2007)
	2.01	1.15	298	0.0	Kung et al (2004)
	0.71	0.71	298	1.0-9.6	Jackson et al. (1999)
	2.75	1.47	298	0.0-10.1	Flesh et al. (1998)
Shearmod	1.00	0.34	294-1073	0.0	Jackson et al (2007
	3.14	1.63	293	0.0-16.8	Kung et al (2004)
	2.68	2.68	298	0.0	Jackson et al (1999)
	2.51	1.75	298	0.0-8.1	Ji et al (1999)
	4.12	1.62	298	0.0-8.8	Flesh et al (1998)
HPClino enstatite					
Volume	0.07	0.05	298	6.5-7.93	Angel & Hugh-Jones (1994)
	0.38	0.21	300	4.0-11.4	Shinmei et al. (1999)
	0.16	0.07	298	6.5-11.7	Kung et al. (2004)
	0.13	0.06	298-1173	6.5-13.0	Kung et al. (2005)
V_P	0.57	0.20	298-1073	6.5-13.0	Kung et al. (2005)
V_S	0.83	0.20	298-1073	6.5-13.0	Kung et al. (2005)
V_B	0.13	0.07	298-1073	6.5-13.0	Kung et al (2005)
LPClino-enstatite					
Volume	0.33	0.15	293-1100	0.0	Hugh-Jones (1997)
	0.10	0.039	293	0.0-7.0	Angel&Hugh-Jones (1994)
	35.0	4.0	100-2000	0.0-8.0	Yu et al (2010, ab initio)
Majorite					
Volume	0.31	0.31	298	0.0	Kato et al. (1985)
	0.51	0.51	298	0.0	Angel et al. (1989)
	0.32	0.32	298	0.0	Matsubara et al. (1990)
	0.22	0.12	298	1.4-9.7	Yagi et al. (1992)
	0.23	0.23	298	0.0	Pacalo et al (1997)
	0.19	0.19	298	0.0	Sinogeikin et al (1997)
α	2.46	1.02	293	0.0-34.0	Suzuki (1983)
	7.23	2.58	0-2500	0.0-30	Yu et al (2011, abinitio)
K_S	3.02	1.52	300-1000	1.6-9.4	Gwanmesia et al (2009,2000)
Shearmod	0.52	0.16	300-1000	1.6-9.4	Gwanmesia et al (2009,2000)
Akimotoite					
Volume	0.30	0.11	298-1373	0.0-18.3	Wang et al. (2004), DO07
	0.56	0.21	298	0.0-27.8	Reynard&Rubie(1996,NaCl)
	0.75	0.20	298	0.0-25.2	Reynard&Rubie(1996,Ice)
	0.27	0.10	298-896	0.0	Ashida et al. (1988)
	0.00	0.00	293	0.0	Horiuchi et al. (1982)

Table 2. (continued)

Property	Max absolute deviation in %	Average absolute deviation in %	*T*-range in K	*P*-range in GPa	Reference
K_S	0.18	0.18	298	0.0	Weidner & Ito (1985)
Shearmod	9.80	9.80	2000	0.0	Li et al (2009, ab-initio)
	0.02	0.02	298	0.0	Weidner & Ito (1985)
Stishovite					
Volume	0.09	0.04	298	0.0-15.8	Ross et al. (1990, DO07)
	0.08	0.04	291-873	0.0	Ito et al. (1974)
	0.13	0.05	298	37.0	Hofmeister (1996, DO07)
	0.45	0.20	300	24.6-49.4	Hemley et al. (1994)
	0.41	0.10	300-1273	0.0-10.0	Liu et al. (1999, NaCl)
	0.28	0.15	300	0.0-29.1	Yamanaka et al.(2002, DO7)
	0.10	0.05	298	0.0-10.0	Andrault et al. (2003, quartz)
	0.51	0.23	298	11.0-47.0	Andrault et al. (2003, NaCl)
	0.39	0.14	298	49.0-121.0	Andrault et al (2003, DO07)
	0.84	0.50	300	2.5-59.2	Panero et al. (2003, MgO, Pt, Ruby)
	0.10	0.03	300-1073	0.0-22.7	Nishihara et al.(2005, DO07)
Shearmod	1.60	1.60	300	0.0	Weidner (1982)
	0.25	0.24	300	0.0-3.0	Li et al (1996)
	2.50	2.50	300	0.0	Brazhkin et al (2005)
	5.06	3.20	300	0.0-12.0	Jiang et al (2009)
	2.06	1.00	300-3000	0.0	Yang et al. (2014)
Perovskite					
Volume	0.02	0.02	298	0.0	Ito & Matsui (1978)
	0.26	0.26	298	0.0	Horiuchi et al. (1987)
	0.24	0.24	298	0.0-9.6	Kudoh et al. (1987)
	0.31	0.21	77-298	0.0	Ross & Hazen (1989)
	0.24	0.09	298	0.0-12.6	Ross & Hazen (1990)
	0.08	0.07	295-404	0.0	Wang et al. (1994)
	0.52	0.16	298-1276	4.3-10.7	Wang et al. (1994)
	0.29	0.13	298-1173	0.0-20.7	Utsumi et al. (1995)
	0.35	0.15	298-2000	25.0	Funamori et al. (1996)
	0.74	0.32	293-2668	26.5-55.7	Fiquet et al. (1998)
	0.69	0.51	298-1357	36.2-109	Saxena et al. (1999)
	0.29	0.14	298	0.0-15.0	Sugahara et al. (2006)
	0.16	0.11	298	0.0-10.0	Van Peteghem et al. (2006)
	0.22	0.11	300-2300	0.0-53.0	Katsura et al (2009)
K_S	5.00	5.00	298	0.0	Yeganeh Haeri et al. (1994)
	0.92	0.92	298	0.0	Sinogeikin et al. (2004)
K_T	3.98	1.69	0-4000	0.0-150	*Tsuchiya et al. (2005)*
V_B	0.55	0.19	298	7.7-96.0	Murakami et al (2007)
V_P	0.19	0.11	298	7.7-96.0	Murakami et al (2007)
V_S	1.03	0.37	298	7.7-96.0	Murakami et al (2007)
Postperovskite					
Volume	0.26	0.08	300-2500	111-145	Guignot et al. (2007)
	1.76	1.61	300	121-151	Ono et al. (2006)$^{(D)}$
	0.97	0.79	300	116-144	Ono et al. (2006)$^{(A)}$
	0.51	0.23	300	111-137	Ono et al. (2006)$^{(J)}$
K_T	7.54	3.22	0-4000	0.0-150	*Tsuchiya et al. (2005)*
V_B	0.23	0.14	0	0.0-130.0	*Tsuchiya et al (2004)*
	1.52	1.52	0	120.0	*Oganov et al (2004)*

Table 2. (continued)

Property	Max absolute deviation in %	Average absolute deviation in %	*T*-range in K	*P*-range in GPa	Reference
V_P	0.86	0.40	0	0.0-130.0	*Tsuchiya et al (2004)*
	1.66	1.66	0	120.0	*Oganov et al (2004)*
V_S	1.39	0.78	0	0.0-130.0	*Tsuchiya et al (2004)*
	1.86	1.86	0	120.0	*Oganov et al (2004)*
Forsterite					
Volume	0.25	0.18	299-1313	0.0	Trots et al (2012)
	0.34	0.17	153-889	0.0	Ye et al (2009)
	0.89	0.28	300-2150	0.0	Bouhifd et al (1996)
	0.09	0.07	130-1300	0.0	Kajiyoshi (1985)
	0.22	0.10	130-1213	0.0	Suzuki (1984)
	0.13	0.08	300	0.0-9.7	Zhang et al (1998)
	0.50	0.32	300	0.0-17.2	Downs et al (1996)
	0.49	0.28	300	3.1-16.2	Zha et al (1996)
K_S	0.61	0.36	300-1300	0.0	Isaak et al (1989)
	0.46	0.26	298-823	0.0	Suzuki et al (1983)
	0.94	0.37	100-700	0.0	Sumino et al (1977)
	0.82	0.43	1.1-12.5	0.0	Li et al (1996)
	4.15	1.82	3.1-16.2	0.0	Zha et al (1996)
Shearmod	0.80	0.30	300-1300	0.0	Isaak et al (1989)
	0.47	0.23	298-1213	0.0	Suzuki et al (1983)
	0.60	0.43	100-700	0.0	Sumino et al (1977)
	0.51	0.26	300	1.1-11.9	Li et al (1996)
	2.25	1.11	300	3.1-16.2	Zha et al (1996)
Wadsleyite (anhydrous)					
Volume	0.05	0.02	297-1100	0.0	Trots et al (2012)
	0.08	0.08	293	0.0	Deon et al (2010)
	0.54	0.25	293-973	0.0	Inoue et al (2004)
	0.29	0.11	293-1073	0.0	Suzuki (1980)
	0.09	0.05	293	0.0-6.4	Holl et al (2008)
	0.50	0.33	293	0.0-10.2	Hazen et al. (2000)
	0.78	0.59	293	0.0-7.6	Meng et al (1993)
	0.63	0.52	293	0.0-4.5	Hazen et al (1990)
α	13.0	3.67	200-1500	0-20.0	*Wu et al (2007)*
K_S	1.65	1.20	300-873	0.0	Li et al (1998)
	0.57	0.42	300	0.0-7.0	Li et al (1998)
	4.22	2.00	300	0.0-14.2	Zha et al (1997)
Shearmod	0.31	0.12	300-873	0.0	Sinogeikin et al (2003)
	0.21	0.10	300	0.0-14.2	Sinogeikin et al (2003)
	2.71	1.41	300-873	0.0	Li et al (1998)
	2.14	1.44	300	0.0-7.0	Li et al (1998)
	2.70	2.39	300	0.0-14.2	Zha et al. (1997)
	2.15	0.96	300	0.0-3.0	Gwanmesia et al (1990)
Ringwoodite (anhydrous)					
Volume	0.62	0.09	133-911	0.0	Ye et al (2009)
	0.32	0.14	293-973	0.0	Inoue et al (2004)
	0.42	0.18	294-1173	0.0	Ming et al (1992)
	0.28	0.09	273-1023	0.0	Suzuki (1979)
	0.46	0.10	300-1900	0.0-22.5	Katsura et al (2004)
α	3.00	1.06	100-2000	0.0	*Yu et al (2006)*
	13.0	4.00	200-2000	21.0	*Yu et al (2006)*

Table 2. (continued)

Property	Max absolute deviation in %	Average absolute deviation in %	*T*-range in K	*P*-range in GPa	Reference
K_S	1.62	1.05	298	12.1	Li et al (2003)
	0.52	0.46	298	12.1	Sinogeikin et al (2003)
	3.63	1.24	298-873	0.0	Jackson et al (2000)
	2.53	1.50	298-873	0.0	Sinogeikin et al (2003)
Shearmod	0.27	0.09	298-873	0.0-12.1	Sinogeikin et al (2003)
	1.08	0.44	298	0.0-12.1	Li et al (2003)
	1.64	0.91	298-873	0.0	Jackson et al (2000)
Periclase (MgO)					
Volume	0.29	0.12	298-2385	0.0	Fiquet et al (1999)
	0.41	0.12	298-2986	0.0	Dubrovinsky et al (1997)
	0.10	0.05	298-1650	0.0-23.6	Kono et al (2010)
	0.86	0.42	298	0.0-90.0	Jacobsen et al (2008)
	0.04	0.04	298	0.0-150.0	Li et al (2006)
	0.67	0.24	298	0.0-52.2	Speziale et al (2001)
	0.34	0.11	298	0.0-54.0	Speziale et al (2001, DO07)
	0.59	0.18	298	0.0-54.1	Zha et al (2000)
	0.22	0.10	298	0.0-23.0	Fei et al (1999)
Volume	1.30	0.57	5700-7300	174.0-203.0	Fatyanov et al (2009)
Hugoniot	0.90	0.33	300-2000	13.8-132.6	Duffy et al (1995)
	0.35	0.26	3081-3663	174.0-203.1	Svendsen & Ahrens (1987)
	1.32	0.75	2600-3800	159.7-199.3	Vassiliou & Ahrens (1981)
	1.07	0.37	300-1800	18.0-122.0	Marsh et al (1980)
K_S	0.68	0.24	295-1073	0.0	Sinogeikin et al (2000)
	0.81	0.64	300-1800	0.0	Isaak et al (1989)
	0.34	0.20	200-1300	0.0	Sumino (1983)
	1.25	0.50	298	0.0-20.8	Kono et al (2010)
	2.30	0.61	298	0.0-11.0	Li et al (2006)
	11.3	3.78	298	0.0-55.0	Zha et al (2000)
	3.40	1.97	298	0.0-18.6	Sinogeikin et al (1999)
	0.50	0.27	298	0.0-30.0	Duffy et al (1995)
Shearmod	1.15	0.44	295-1073	0.0	Sinogeikin et al (2000)
	2.00	0.68	300-1800	0.0	Isaak et al (1989)
	1.48	0.54	200-1300	0.0	Sumino (1983)
	1.77	0.57	298	0.0-20.8	Kono et al (2010)
	1.08	0.44	298	0.0-11.0	Li et al (2006)
	16.6	4.37	298	0.0-55.0	Zha et al (2000)
	0.66	0.26	298	0.0-18.6	Sinogeikin et al (1999)
	4.94	1.76	298	0.0-30.0	Duffy et al (1995)

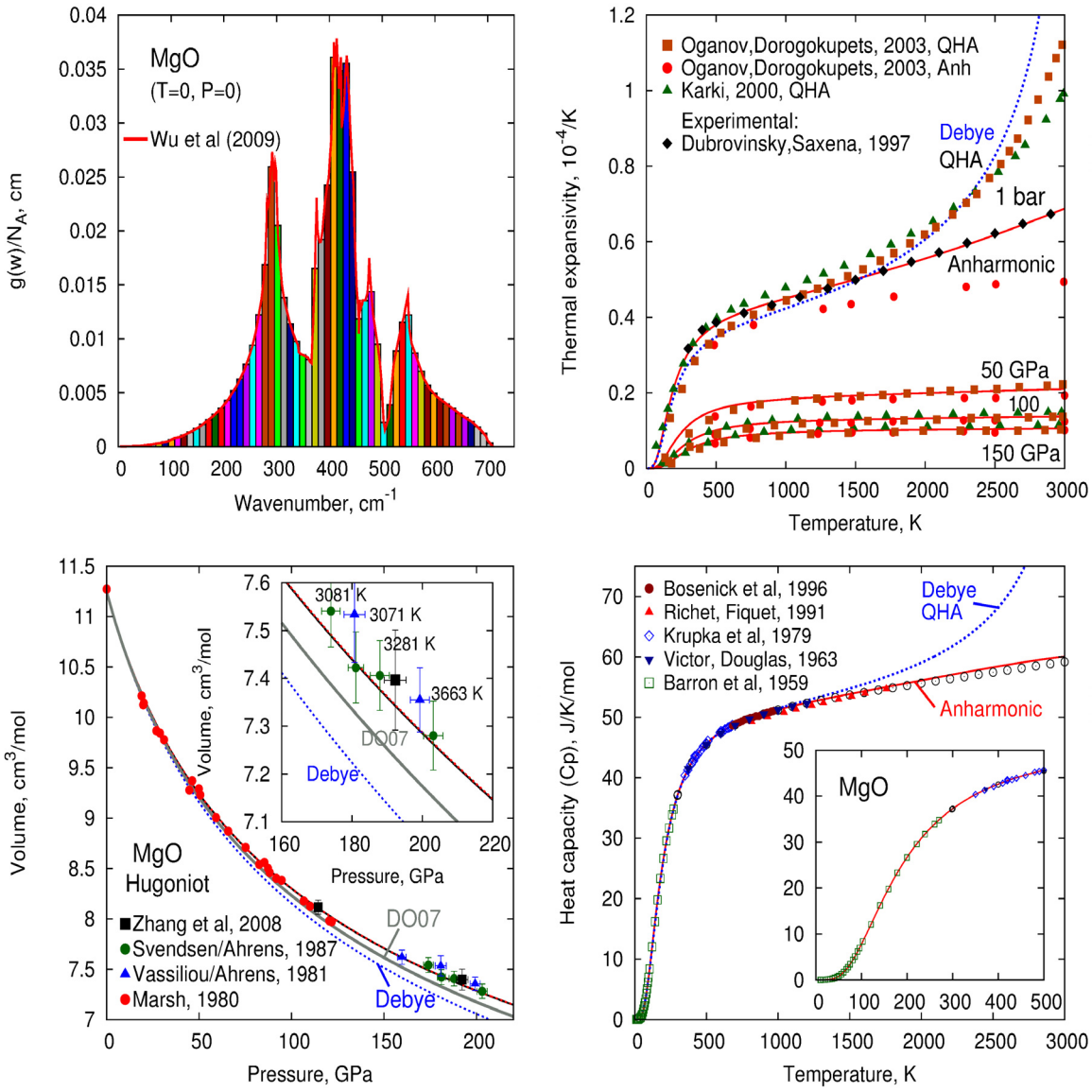

Fig. 1. Thermodynamic properties calculated with a database in which the VDoS of MgO is represented by 60 Einstein frequencies are insignificantly different from those calculated with a database in which the VDoS is represented by 1 Einstein frequency. Upper-left: VDoS represented by 60 Einstein continua. Upper-right: thermal expansion calculated with Einstein models plotted as solid curves. The dashed curve was calculated for 1 bar with the Debye model of Stixrude and Lithgow-Bertelloni (2011). At high pressures the anharmonic Einstein model converges to a quasi-harmonic model. Lower-left: Hugoniot calculated with Einstein models. The blue dashed curve was calculated with the Debye model of Stixrude and Lithgow-Bertelloni (2011). The grey curve results from the MgO description of Dorogokupets & Oganov (2007). Lower-right: heat capacity using Einstein models plotted as the solid curves compared with the Debye model by Stixrude and Lithgow-Bertelloni (2011) plotted as the dashed curve. Open circles are not experimental points but result from an extrapolation by Barin (1987)

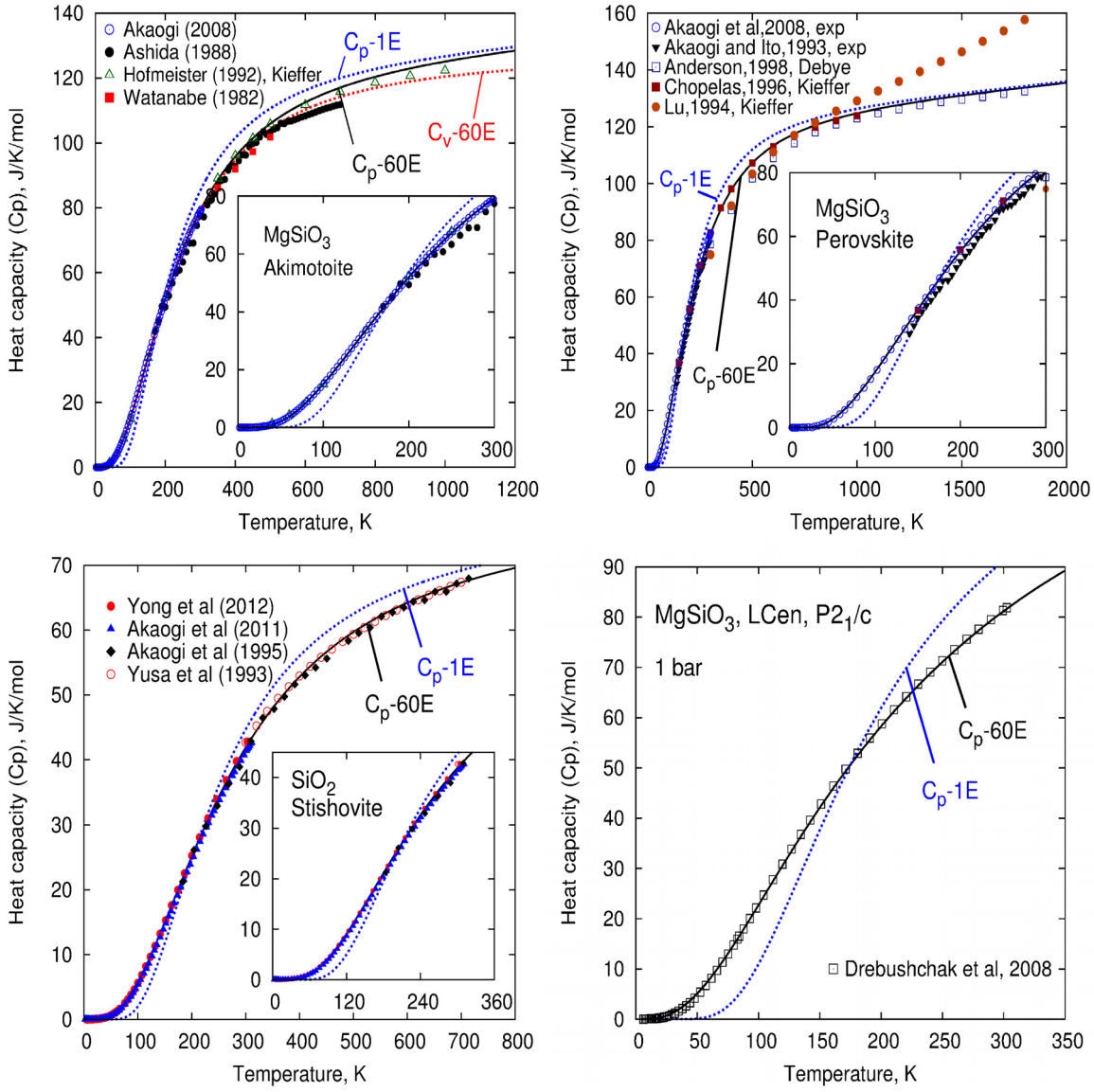

Fig. 2. Heat capacity for four phases. Curves labelled C_p-60E (C_v-60E) denote isobaric (isochoric) heat capacity calculated with the database in which the VDoS of each polymorph is represented by 60 Einstein frequencies. The dashed curves labelled C_p-1E denote heat capacity calculated with a clone in which the VDoS is represented by one Einstein frequency. Upper-left: the triangles of Hofmeister (1992) are the result of a calculation using Kieffer's (1979) model. Upper-right: Investigators labelled with 'exp' denote experimentally determined heat capacity. Other investigators used a Debye model or Kieffer model

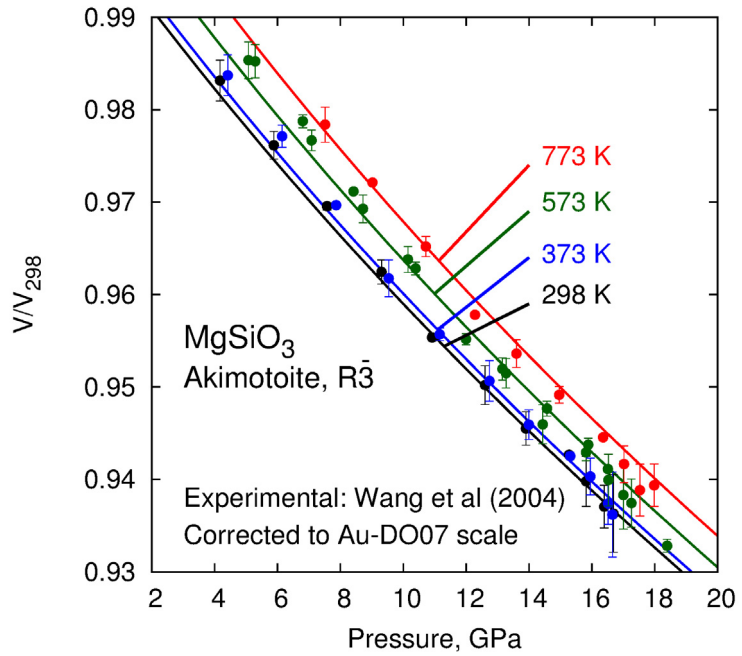

Fig. 3. Isotherms for akimotoite. Experimental data measured by Wang et al. (2004) based on Anderson's (1989) gold scale were converted to the gold pressure scale of Dorogokupets & Oganov (2007). The last scale gives about 0.5 GPa larger pressures at about 16-18 GPa compared to Anderson's scale. Data from Reynard (1996a) at 300 K are consistent with the data of Wang et al. (2004), but not plotted for the sake of transparency